Full Text View

Volume 28, Issue 2 (February 1998)

Journal of Physical Oceanography
Article: pp. 309–321 | Abstract | PDF (245K)

The Formation of Estuarine Turbidity Maxima Due to Density Effects in the Salt Wedge. A Hydrodynamic Process Study

Hans Burchard

International Research Centre for Computational Hydrodynamics, Danish Hydraulic Institute, Hørsholm, Denmark

Helmut Baumert

Institut für Meereskunde, Universität Hamburg, Hamburg, Germany

(Manuscript received August 19, 1996, in final form June 6, 1997)

DOI: 10.1175/1520-0485(1998)028<0309:TFOETM>2.0.CO;2

ABSTRACT

By means of a numerical model of an idealized flat-bottom estuary, the paper studies the hydrodynamic control of the turbidity zone by the combined effect of the salt wedge and tidal movements. The model is of two- dimensional (x, z) finite-difference type with high resolution in time and space. It computes momentum, surface elevation, salinity, suspended particulate matter (SPM), turbulent kinetic energy, and dissipation rate as prognostic state variables. At the seaward boundary a tidal forcing is applied. At the landward boundary a weir is situated where a constant freshwater discharge is prescribed. The initial SPM concentration is horizontally homogeneous. After simulating a few tidal periods the model results exhibit the evolution of a stable SPM peak (the estuarine turbidity maximum or ETM) at the tip of the salt wedge. An inspection of the tidal mean velocity profiles around the ETM shows that this trapping of SPM is due to a residual near-bottom upstream current in the region of the salt wedge. Three physical causes for this residual countercurrent are investigated in greater detail by numerical experiments, namely, (i) the *residual gravitational circulation,* (ii) the *tidal velocity asymmetry,* and (iii) *the tidal mixing asymmetry.* The first mechanism is related to the baroclinic part of the longitudinal pressure gradient. The second and third mechanism are based on the differences between the vertical profiles of velocity and SPM, respectively, at flood and ebb tide. For the macrotidal estuary considered here, the consideration of both (i) and (ii) could be shown to be *necessary* for the establishment of an ETM in the considered idealized estuary. It could further be shown that (iii) affects the ETM formation only quantitatively but not qualitatively and appears to be not necessary for the existence of an ETM.

Table of Contents:
- Introduction
- Physical equations
- Discretization
- Numerical experiments
- Results and discussion
- Conclusions
- REFERENCES
- TABLES
- FIGURES

1. Introduction

Estuaries act in a sense as a link between the limnetic and marine environments and are thus characterized by a variety of complex and complicated processes (Michaelis 1990). One typical and very important estuarine phenomenon is the frontal zone between the fresh and saline water. In many macrotidal estuaries this front can be characterized by a salt wedge moving horizontally with the semidiurnal tidal cycle. In a wide range of those estuaries, stable turbidity maxima can be observed at the tip of the salt wedge (see, e.g., Wellershaus 1981). These estuarine turbidity maxima (ETM) are formed by high concentrations of suspended particulate matter (SPM) that trigger to a large extent the functioning of estuarine ecosystems [see, e.g., Simenstad et al. (1994) for the Columbia estuary, Kausch and Michaelis (1996) for the Elbe estuary in Germany, and Le Bris and Glémarec (1996) for the Lorient and Vilaine Bays in Brittany].

Strong correlations between the locations of turbidity maxima and high loads of fluid mud (particle size <0.063 mm, density 1.2–1.4 g cm^{-3}) close to the bottom of the estuary have been observed (Dammschneider 1992). Two interpretations are possible: (i) the fluid- mud maximum (i.e., the bottom deposit of the SPM) is the cause for the ETM farther up in the water column (e.g., Lang 1989) and (ii), vice versa, the ETM is governed by other effects and represents the cause for the bottom deposit of SPM.

If the latter is the case, then a better understanding of ETM dynamics would be of great practical relevance for the design of dredging strategies in macrotidal estuaries. In the present paper we adopt this latter position and show by numerical experiments that in macrotidal estuaries an ETM is formed fully independent from near-bottom deposits of SPM or fluid mud, only by hydrodynamic effects.

The formation of an ETM is not easy to understand. If one concentrates on physical mechanisms only [flocculation and deflocculation and several processes connected to the ionic composition of water are modulating the ETM dynamics, e.g., see Postma and Kalle (1955);Wellershaus (1981); van Leussen (1988)], then one has to accept the following argument. As a consequence of a permanent freshwater discharge from the headwater into the estuary there is a tidal-mean residual freshwater flow out of the estuary into the sea, which has a tendency to wash out all suspended and dissolved material from the estuary. Therefore, one has to look for a mechanism that counteracts the outflow transport of SPM, that is, for a countercurrent that transports the SPM in the landward direction, up to reaching a steady-state situation in which this countercurrent is balanced by the freshwater outflow. Such near-bottom residual countercurrents have explicitely been measured just recently by Lindsay et al. (1996) in the Forth estuary (Scotland). During spring tide, the residual countercurrents were observed to be of the order 0.1 m s^{-1} and coincided with landward fluxes of SPM.

In this paper, among the possible physical mechanisms for a countercurrent, we concentrate on joint numerical modeling of the following three, which are related to the salt wedge and have been described by other authors in the literature:

1. *Residual gravitational circulation.* In the vicinity of the (continuous) salt wedge a significant longitudinal baroclinic pressure gradient exists that forces the near-bottom horizontal velocity permanently upstream, while the freshwater outflow forces the upper-layer velocity permanently downstreams. In the vicinity of the tip of the wedge, where the longitudinal baroclinic pressure gradient is strong enough, this mechanism leads to a gravitational circulation (in the tidal mean: to a residual circulation) within the vertical plane. This effect was first suggested by Postma and Kalle (1955) and since then is known to be one major driving force for ETM [see the stationary numerical experiments by Festa and Hansen (1976, 1978)]. The presence of tides is not neccessary for this mechanism.

2. *Tidal velocity asymmetry.* Due to the convective instability of the near-bottom flow at flood tide (fast salty layers moving over slow layers of brackish or freshwater), the vertical velocity profile is much more uniform at flood than at ebb tide. As a consequence, velocity profiles are bottom intensified during flood and surface intensified during ebb. Because the SPM concentration usually always increases toward the bottom, this velocity asymmetry at flood and ebb can lead to an upstream net transport of SPM. This effect was first discussed by Jay and Musiak (1994) by means of approximate analytical considerations.

3. *Tidal mixing asymmetry.* Due to the stable stratification of the ebb current (fast freshwater at the surface moves over slow salty layers at the bottom), vertical mixing is suppressed at the density interface such that almost all SPM is kept below that interface in the region of slow velocities. As a consequence we can have again an upstream net transport of SPM. This mechanism has been proposed first by Geyer (1993) who extended the stationary numerical experiments carried out by Festa and Hansen (1976, 1978) to the stratified case.

Some other possibly relevant mechanisms of ETM formation have been described in the literature, too. They are mainly of barotropic or topographic nature. See, for example, Fischer (1972), Ionello (1979), Allen et al. (1980), and van de Kreeke

(1996).

The major aim of this paper is to provide a first qualitative time-dependent comparison of these three mechanisms in an idealized approach that contains the full relevant physics. In the following, the above mechanisms (1), (2), and (3) are investigated for macrotidal estuaries by means of a time-dependent, flat-bottom, shallow-water model in alongstream and vertical coordinates (a spatially two-dimensional model). This type of model is well established in investigations of density-driven currents and can today be justified by the same arguments as by Ariathura and Krone (1976): "Although estuarine flows are generally three-dimensional in nature, in most cases averaging over the . . . width can provide a great deal of useful information. Until two-dimensional models have reached a greater degree of sophistication, the effort required to develop a three- dimensional model does not seem to be warranted. . . ." The particular advantage of such an idealized 2D model in comparison to fully 3D models with realistic topography [see, e.g., the 3D SPM model by Lang et al. (1989) for the Weser estuary] is that it allows one to focus on only a few relevant physical processes and to use the necessary fine vertical resolution. A coarse vertical resolution typical for 3D models may be a reason for the problems of such models in representing the setup of ETM (see Lang et al. 1989).

2. Physical equations

We consider in the *xz*-plane a two-dimensional channel of length L and constant bottom coordinate at $z = -H$, where x is the horizontal and z the vertical (upward) coordinate; ζ is the free surface elevation, and u and w are the horizontal and vertical velocity, respectively. The channel has an open boundary at $x = 0$ and a closed boundary (a weir) at $x = L$.

a. Balance of water mass and momentum

The basic hydrodynamic equations are the incompressibility condition

$$\partial_x u + \partial_z w = 0, \quad (1)$$

the momentum equation

$$\partial_t u + \partial_x(u^2) + \partial_z(wu - (\nu + \nu_t)\partial_z u) = -\frac{1}{\rho_0}\partial_x p, \quad (2)$$

and the hydrostatic assumption

$$\partial_z p + g\rho = 0, \quad (3)$$

where p is the pressure, ρ the density, ρ_0 a constant reference density, g the gravitational acceleration, ν the kinematic viscosity, and ν_t the vertical eddy viscosity.

At the surface and at the bottom, kinematic boundary conditions are given:

$$w = \partial_t \zeta + u\partial_x \zeta \quad (4)$$

for $z = \zeta$ and

$$w = 0 \quad (5)$$

for $z = -H$. Integration of (1) under consideration of (4) and (5) yields the surface elevation equation,

$$\partial_t \zeta = -\partial_x \int_{-H}^{\zeta} u \, dz. \quad (6)$$

By means of integrating (3) vertically and assuming horizontally homogeneous atmospheric pressure, an expression for the horizontal pressure gradient can be derived:

$$-\frac{1}{\rho_0}\partial_x p(z) = -g\frac{\rho(\zeta)}{\rho_0}\partial_x \zeta - \frac{g}{\rho_0}\int_z^{\zeta} \partial_x \rho(\xi)\, d\xi. \quad (7)$$

The first term on the right-hand side of (7) is referred to as the external and the second term as the internal or baroclinic pressure gradient. It is the latter pressure gradient that is shown below to be responsible for the *residual gravitational circulation* mentioned in mechanism (i) above.

Throughout this paper, the density is assumed to be a function of salinity only. This simplification is reasonable in most estuaries where the effect of SPM concentrations and temperature on density are small compared to the dominating salt wedge. Here, for convenience we assume a constant water temperature of $T = 10°C$ and apply the following quadratic approximation to the UNESCO density formula (see Gill 1982), which is exact at $S = 5$ psu, $S = 15$ psu, and $S = 25$ psu:

$$\rho = \rho_0(1 + aS + bS^2) \quad (8)$$

with $a = 7.7759 \times 10^{-4}$ and $b = -3.351 \times 10^{-9}$.

b. Hydrodynamic boundary conditions

At the bottom of the estuary we assume the existence of a logarithmic boundary layer (LBL) in which the shear stress is constant and the eddy viscosity proportional to the distance from the bottom. According to Baumert and Radach (1992), the bottom stress can be modeled as

$$\nu_t \partial_z u = \frac{\tau_b}{\rho_0} = u_* |u_*| = ru|u| \quad (9)$$

for $z \in$ LBL with the bottom friction velocity u_*, the bottom drag coefficient

$$r(z) = \frac{\kappa^2}{\ln^2\left(30\frac{\tilde{z}}{K_s}\right)}, \quad (10)$$

the roughness length K_s, the von Kármán constant $\kappa = 0.4$, and $\tilde{z} = K_s/30 + z + H$. No wind forcing is assumed, which leads to zero surface stress:

$$\nu_t \partial_z u = \frac{\tau_s}{\rho_0} = 0, \quad (11)$$

at $z = \zeta$. The hydrodynamic equations are forced by means of a radiation condition at the open boundary at $x = 0$ (see Flather 1976);

$$u(z, t) = u_T(t) + \frac{\sqrt{gD(t)}}{D(t)}(\zeta_T(t) - \zeta(t)), \quad (12)$$

with

$$\zeta_T(t) = \zeta_0 \cos\left(\frac{2\pi t}{T}\right) \quad (13)$$

and

$$u_T(t) = u_0 \cos\left(\frac{2\pi(t - t_0)}{T}\right), \quad (14)$$

where $D = (\zeta + H)$ is the total water depth, T the period of the M_2 tide, and u_0 and ζ_0 the amplitudes of the surface elevation and velocity forcing functions respectively; t_0 is the time lag of the velocity forcing function with respect to ζ_T. The boundary condition (12) generates tidal waves propagating into the domain, while waves from inside can leave the domain with minimal reflections. Due to the nonlinearities in the model, the surface elevation curve at $x = 0$ includes higher

harmonics like the M_4 period, although the forcing functions u_T and ζ_T only contain the M_2 frequency.

At the weir ($x = L$), a constant freshwater discharge is prescribed:

$$u(z, t) = u_r \frac{H}{D(t)} \qquad (15)$$

at $x = L$. Here u_r is the mean cross-sectional runoff velocity.

Obviously, the longitudinal Dirichlet boundary conditions (12) and (15) for $u(x, z, t)$ do not depend on the vertical location within the boundary water columns. That is, we assume vertical homogeneity or, in other words, a vertical wavenumber that equals zero. Due to the dominance of friction, these artificial conditions become neutralized very close to the boundary columns. On the other hand, this specific approach avoids the boundary value problem (1)–(3) being ill-posed [for details of this interesting mathematical problem see Browning et al. (1990)].

c. Salinity

The transport equation for salinity has the form:

$$\partial_t S + \partial_x(uS) + \partial_z(wS - (\nu' + \nu'_t)\partial_z S) - \mathcal{A} = 0, \qquad (16)$$

where ν' is the molecular diffusivity and ν'_t the vertical eddy diffusivity.

The term $\mathcal{A}$ models lateral dispersion and exchange processes in the seaward domain of the estuary:

$$\mathcal{A} = c_m u^+ (x_m - x)^+ (S_{\max} - S). \qquad (17)$$

Here, c_m is a constant, x_m the fixed upstream end of this domain, and $S_{\max}$ the maximum salinity. The notation $X^+ = (X + |X|)/2$ for any quantity X is an abbreviation. The term $\mathcal{A}$ represents a kind of bulk parameterization of diverse differential transport phenomena in an estuarine cross section. In the framework of the present two-dimensional model concept, $\mathcal{A}$ is necessary in order to establish a stable and smooth salt wedge that is moving up- and downstream with the tides according to the observations. The term $\mathcal{A}$ acts only in the region close to the open sea boundary during flood. A background longitudinal dispersion due to cross-sectional flow variability and tidal chaos, effects associated with bottom topography and curvatures in real estuaries, is considered here only in a bulk sense by an effective diffusion coefficient. Specifically, the grid size is chosen such that the effective numerical diffusion in the longitudinal direction obeys the same order of magnitude as in the Elbe estuary (namely, about 120 $m^2\ s^{-1}$, see section 3).

At the open longitudinal boundaries, the following Dirichlet conditions for salinity are chosen. At the seaward end for inflow conditions ($u > 0$), seawater with maximum salinity ($S = S_{\max}$ at $x = 0$), and at the riverine end (the weir) freshwater with zero salinity ($S = 0$ at $x = L$) is advected into the estuary.

At the surface and the bottom, zero flux conditions for salinity are applied:

$$(\nu' + \nu'_t)\partial_z S = 0 \qquad (18)$$

for $z = \zeta$ and for $z = -H$.

d. SPM dynamics

The SPM is considered here as a continuous quantity and is described by its concentration C [kg SPM m^{-3}]. For the sake of simplicity we assume that all SPM flocs, particles, or aggregates have the same size and consistency and therefore the same sinking velocity, w_s, constant in space and time. Processes like the aggregation/destruction of flocs and their consequences for the variability of the sinking velocity (e.g., hindered settling) are beyond the scope of this paper and are supposed to modify the results quantitatively but do not introduce a new ETM formation mechnism in principle. The SPM particles are assumed to be noncohesive. Further, we restrict these considerations to the case of relatively small SPM concentrations such that the effects of the SPM on the fluid density, and therefore on the flow and pressure dynamics, can

be neglected. With these assumptions the SPM transport equation simply reads

$$\partial_t C + \partial_x(uC) + \partial_z((w - w_s)C - (\nu'' + \nu_t')\partial_z C) = 0. \quad (19)$$

It is the turbulent mixing term $\nu_t' \partial_z C$ in this equation that is responsible for the *tidal mixing assymmetry* mentioned as mechanism (iii).

At the lateral boundaries of the estuary, homogeneous Neumann conditions for the SPM are given for inflow conditions:

$$\partial_x C = 0 \quad (20)$$

for $x = 0$ and for $x = L$. No SPM flux through the surface is assumed:

$$w_s C + (\nu'' + \nu_t')\partial_z C = 0 \quad (21)$$

for $z = \zeta$. The SPM flux through the bottom is the result of erosion F_e and sedimentation F_s:

$$-w_s C - (\nu'' + \nu_t')\partial_z C = F_e - F_s \quad (22)$$

for $z = -H$. The existence of a bed layer is assumed in which nondynamic particulate matter (PM) lays at rest. This PM pool B is filled and emptied by sedimentation and erosion, respectively:

$$\partial_t B = F_s - F_e \quad (23)$$

so that the conservation of SPM per unit length of the estuary is guaranteed. Following Krone (1962) (see also Ariathurai and Krone 1976), erosion and sedimentation are modeled as nonnegative functions of the bottom shear stress τ_b and critical shear stresses τ_{ce} and τ_{cs}. Both are limited, F_e by the PM pool in the bed layer B and F_s by the near-bottom SPM concentration C_b:

$$F_e = \begin{cases} \frac{c_e}{\rho_0}(|\tau_b| - \tau_{ce})^+ & \text{for } B > 0 \\ 0 & \text{elsewhere} \end{cases} \quad (24)$$

and

$$F_s = \frac{w_s C_b}{\tau_{cs}}(\tau_{cs} - |\tau_b|)^+, \quad (25)$$

where c_e is a proportionality factor. Notice that the pool B has finite size with respect to erosion: It can only be eroded to what has been settled before or what was already part of the pool initially.

e. Turbulence model

Turbulence plays a complex and complicated key role in the overall dynamics of the estuarine system because it has an influence on nearly all scales and processes. Therefore, a good representation of turbulence is needed for the present model. We have chosen here the two- equation k–ε turbulence closure (see Launder and Spalding 1972; Rodi 1980) because models of this type have been successfully applied to a variety of geophysical flows in the last 20 years (see, e.g., Marchuk et al. 1977; Omstedt et al. 1983; Rodi 1987; Baumert et al. 1989; Baumert and Radach 1992; Brøers and Eidsvik 1994; Burchard and Baumert 1995). A major advantage of such two-equation turbulence models in comparison to simpler algebraic turbulence parameterizations based on an turbulence equilibrium assumption is the consideration of time lag effects between mean current and turbulence (see Schröder and Siedler 1980; Baumert and Radach 1992), which might play an important role in sediment dynamics. Another benefit of two-equation models is their numerical robustness (see Burchard and Baumert 1995).

In k–ε models, k is the turbulent kinetic energy (TKE) and ε the dissipation rate of the TKE. In the following, the advective terms in the turbulence equations will be neglected. This seems to be admissible because in the largest parts of the

salt wedge the vertical gradients of these quantities are much stronger than the horizontal gradients. Therefore, the transport equations for k and ε are used in the following form:

$$\partial_t k - \partial_z\left(\frac{\nu_t}{\sigma_k}\partial_z k\right) = P + G - \varepsilon \qquad (26)$$

and

$$\partial_t \varepsilon - \partial_z\left(\frac{\nu_t}{\sigma_\varepsilon}\partial_z \varepsilon\right) = c_1\frac{\varepsilon}{k}(P + c_3 G) - c_2\frac{\varepsilon^2}{k}. \qquad (27)$$

Here

$$P = \nu_t S^2, \qquad G = -\nu_t' N^2 \qquad (28)$$

are the shear and the buoyancy production of the TKE, respectively. The buoyancy production G is responsible for both the *tidal velocity asymmetry* and the *tidal mixing asymmetry* mentioned in relation with mechanisms (ii) and (iii) (see above). In (28),

$$S^2 = (\partial_z u)^2, \qquad N^2 = -\frac{g}{\rho_0}\partial_z \rho \qquad (29)$$

denote the shear and the Brunt–Väisälä frequency. With the relation of Kolmogorov and Prandtl,

$$\nu_t = c_\mu\frac{k^2}{\varepsilon}; \qquad \nu_t' = c_\mu'\frac{k^2}{\varepsilon} \qquad (30)$$

the system is closed. In the standard model used here, the stability functions c_μ and c_μ' read c_μ = const and

$$c_\mu' = c_\mu\frac{(1 + 10\mathrm{Ri})^{1/2}}{(1 + 3.33\mathrm{Ri})^{3/2}}, \qquad \mathrm{Ri} \geq 0,$$
$$c_\mu' = c_\mu, \qquad \mathrm{Ri} < 0, \qquad (31)$$

(see Munk and Anderson 1948; Rodi 1980), where Ri is the gradient Richardson number, a dimensionless measure of the stability of stratification, given by $\mathrm{Ri} = N^2/S^2$.

The boundary conditions for k and ε are derived from the assumption $P = \varepsilon$ in the vicinity of walls (see Baumert and Radach 1992). Due to the neglect of advection in the k and ε equations, no lateral boundary conditions have to be specified.

The value for c_3 that determines the dampening effect of stratification on turbulence is a matter of discussion in literature (Rodi 1987). In a recent publication (Burchard and Baumert 1995), this empirical constant has been calibrated to $c_3 = -1.4$ for the standard model applied here. All other parameters of the standard model are given in Table 1.

3. Discretization

For the numerical treatment of the full system of model equations a staggered grid with equidistant horizontal and vertical mesh sizes Δx and Δz are used. For the time step a constant Δt has been applied. For the numerical experiments presented here, a fine spatial resolution with Δx = 200 m and Δz = 0.5 m was used. The time step in all calculations was $\Delta t = T/800 \approx$ 56 s.

In order to allow a near-surface resolution that is fine compared to the tidal range, a momentum and mass conserving flooding and drying algorithm for the surface boxes is implemented. As a consequence of this procedure, adjacent surface boxes do not always fit horizontally (see Fig. 1). In those cases, horizontal fluxes have to be calculated carefully (for details, see Burchard 1995). A vertical grid similar to the one used here has been suggested by Casulli and Cheng (1992).

The discrete values for ζ, u, S, C, k, and ε are temporally synchronized: they all are computed for the same instants of

time. The vertically integrated horizontal velocity in the surface elevation equation (6) and the barotropic pressure gradient (7) for the momentum equation are taken central in time. This leads to an implicit system for the surface elevation and the vertically integrated horizontal velocity, which is solved similarly to the procedure described in Backhaus (1985). In the two-dimensional case presented here, a horizontal tridiagonal system for the surface elevation has to be solved. As a consequence of this semi-implicit approach, the time step Δt is not limited by the celerity of the external gravity waves.

For u, S, and C, the vertical diffusive fluxes [including the sinking term in the SPM equation (19)] are calculated central in time; for k and $\mathfrak{E}$ they are taken fully implicit for stability reasons. This leads to a tridiagonal linear system for each quantity in each horizontal discretization point for each time step. In order to guarantee positivity for k and $\mathfrak{E}$, the sink terms on the right-hand side of (26) and (27) are calculated quasi-implicitely (see Patankar 1980). All other terms including the baroclinic pressure gradient are taken explicitly, that is, on the old time level (see Backhaus 1985).

The advection terms in the u, S, and C equations are discretized with a conservative first-order upstream scheme. Except for the costly nonlinear flux-corrected transport schemes (see, e.g., Zalesak 1979), this is the only advection scheme that guarantees both monotonicity and mass conservation. The maximum numerical diffusion coefficients for the longitudinal motion can be estimated as $A^H_{\max} \approx 0.5 u_{\max} \Delta x$, which gives here for $u_{\max} \approx 1.2$ m s^{-1} a value of $A^H_{\max} \approx 120$ m^2 s^{-1}. This numerical diffusion models well the different longitudinal dispersion effects mentioned in section 2c. The maximum vertical numerical diffusion coefficient $A^V_{\max} \approx 0.5 w_{\max} \Delta z$ is with $w_{\max} \approx 2 \times 10^{-4}$ m s^{-1} (the value is so small due to the flat bottom) only $A^V_{\max} \approx 5 \times 10^{-5}$ m^2 s^{-1}, a value that is negligible compared to the maximum physical eddy viscosity of $\nu'_t \approx 5 \times 10^{-2}$ m^2 s^{-1}. With the given maximum velocities, $u_{\max}$ and $w_{\max}$, the maximum estimates of the associated corresponding Courant numbers are $C^u = u_{\max} \Delta t / \Delta x \approx 0.34$ and $C^w = w_{\max} \Delta t / \Delta z \approx 0.02$, which guarantee stable numerical solutions for the explicit advection schemes. The Courant number for the external gravity waves is $C^\zeta = (gH)^{1/2} \Delta t / \Delta x \approx 3.4$, which is admissible due to the implicit treatment of the free surface.

For more details concerning the discretization of the equations see Burchard (1995).

4. Numerical experiments

In order to analyze the driving mechanisms of ETM formation, four numerical experiments have been carried out where the first one serves as a reference with the full physics included as described above.

In each of the other three experiments one basic physical process has been omitted. This is done in order to investigate the relevance of the three ETM mechanisms mentioned in the introduction, namely, (i) the residual gravitational circulation, (ii) the tidal velocity asymmetry, and (iii) the tidal mixing asymmetry.

For all the experiments, we used the same set of physical parameters given in Table 2. The parameters for the tidal forcing, river runoff, and depth are typical for a macrotidal estuary like, for example, the Elbe in northern Germany. The critical shear values τ_{ce} and τ_{cs} for the SPM model are based on the work by Lobmeyr and Puls (1991).

The following four experiments have been carried out:

1. *Experiment 1.* In this reference experiment, the complete set of physical equations described above is included.

2. *Experiment 2.* Here the impact of longitudinal density variations in time and space on the pressure is neglected by omitting the baroclinic pressure gradient from the system. This is realized by setting all density values in (7) equal to the reference density, that is, $\rho = \rho_0$. This experiment allows the study of effect (i), the *residual gravitational circulation.*

3. *Experiment 3.* In this experiment, the impact of density stratification on turbulence is neglected by setting $G = 0$ in the k and the $\mathfrak{E}$ equation, (26) and (27) respectively. Now the enhancement of turbulence by unstable and the damping of turbulence by stable stratification is excluded, with all consequences for the turbulent mixing processes, that is, for the mixing of momentum, turbulence quantities, salinity, and SPM. By means of this experiment, the relevance of (ii) the *tidal velocity asymmetry* on SPM dynamics can be investigated. It should be noted that the (iii) *tidal mixing asymmetry* is only partially excluded here because the effect of density stratification on the stability function c'_μ is still present.

4. *Experiment 4.* In order to test the effect (iii) of the *tidal mixing asymmetry* on the ETM dynamics seperately, in this

experiment only the turbulent vertical exchange in the SPM equation (19) is manipulated as follows: instead of ν'_t computed by the complete turbulence model, a reasonable but constant value ν'_0 (see Table 2) is taken as the vertical eddy diffusivity for SPM (in all other equations the turbulent diffusivities are used). It is well known that this (together with the constant sinking speed w_s) leads to an exponential profile for the vertical SPM distribution, which is only weakly modified by advection.

Each of the aforementioned experiments is initialized with a periodically stationary solution for the whole set of equations neglecting the SPM dynamics. For experiments 1–3, different periodically stationary solutions will be expected. They are obtained by integrating the equations for each of these three experiments over 20 tidal periods. After this initializing phase, the full models including SPM dynamics were integrated over 30 tidal periods. Zero SPM concentration in the water and a horizontally homogeneous value B_0 for the PM pool in the bed have been chosen as initial conditions for SPM.

5. Results and discussion

The results for experiments 1–4 are shown in Figs. 2–9.

a. Experiment with complete physics

The general physical performance of this basic experiment (after a periodically steady state is reached) is illustrated in Fig. 2, which shows instantaneous snapshots of salinity and SPM for different tidal phases. A relatively narrow area of longitudinal salinity gradient is moved back and forth with the tide, stretched during ebb and compressed during flood. In this area, a permanent stratification is present. As a consequence of zero surface stresses (no wind forcing), the highest salinity (and therefore density) gradients occur near the surface. An ETM placed at the upstream end of the salt intrusion follows the tidal motion. Significant surface SPM concentrations only occur at a position of low salinity (<2 psu) where vertical density stratification is weak. During and after flood, the lower half of the water column is homogeneous with respect to salinity and SPM. In contrast to that, both quantities show gradients even close to the bottom during ebb. After ebb, the SPM content of the water column reaches a minimum. However, due to the small sinking speed (w_s = 1 mm s^{-1} = 3.6 m h^{-1}), the ETM is permanently present.

The formation process of the ETM in this basic experiment is demonstrated in Fig. 3a where the vertically averaged tidal mean SPM concentration is shown. After only a few tidal periods, most of the SPM content is concentrated at the upstream tip of the salt wedge. The SPM concentration at the open sea boundary decreases rapidly. Obviously, parts of the SPM content in the lower estuary leave the estuary through the open sea boundary and parts are transported upstream toward the ETM. In the region upstream of the ETM (50 km < x < 75 km), the SPM is advected downstream toward the ETM. The very low SPM concentrations near the river boundary (x > 75 km) even during the first tidal periods are due to the weak bottom stress τ_b, which does not exceed the critical value τ_{ce} [see Eq. (24)].

The vertically averaged tidal mean SPM concentration converges to a steady state with a maximum value of 0.084 kg m^{-3} at x = 35.5 km. There, the vertically averaged tidal mean salinity is S_m = 5.87 psu. Defining the extension of the ETM by means of a vertically averaged tidal mean SPM concentration of 1% of the maximum value, the upstream end is at x = 50.5 km (S_m = 0.00144 psu) and the downstream end at x = 24.5 km (S_m = 20.09 psu), which is outside the open boundary area defined by x_m in (17).

Figure 4 shows tidal mean profiles of horizontal velocity in the lower part of the estuary. It is physically clear for this periodically stationary case that the vertical mean of the residual current equals the prescribed freshwater discharge velocity, which is in this case u_r = 0.05 m s^{-1} (in the downstream direction). But in the vicinity of the largest horizontal gradient of the vertically averaged tidal mean salinity, an upstream residual transport near the bottom can be observed. The maximum value of this transport is larger than 0.05 m s^{-1}. The maximum upstream extension of this residual countercurrent is at x = 38 km. As a consequence of the increase of SPM concentration near the bottom, a residual upstream flux of SPM is resulting (see Fig. 5, where a near-bottom upstream residual flux of SPM can be observed at x = 35 km). It is obvious that an increase of the sinking speed w_s would lead to higher concentrations of SPM near the bottom and therefore to a more efficient blocking of SPM downstream flux. On the other hand, small values of w_s would lead to a more homogeneous SPM distribution in the vertical with the consequence of increased SPM downstream flux.

A comparison of the velocity profiles at maximum flood and ebb shows that the flood profile is bottom intensified

whereas the ebb profile is more stretched (see Fig. 6). This asymmetry that results in the near-bottom residual countercurrent may be generated by (i) residual gravitational circulation as well as by (ii) tidal velocity asymmetry. The latter effect can be explained according to Fig. 6. During flood, a near-bottom unstable salinity stratification is generated due to bottom shear. This leads to an enhancement of vertical mixing near the bottom, which itself decreases the velocity shear and increases the bottom velocity during the flood. The opposite happens during ebb: A bottom shear-induced stable salinity stratification suppresses vertical mixing, which leads to stretched velocity profiles with a smaller bottom velocity.

The principle of the (iii) tiding mixing asymmetry can be demonstrated by means of Fig. 6. As a consequence of the reduced diffusivity during ebb and the enhanced diffusivity during flood, high SPM concentrations are mixed much higher into the water column in the latter case. This generates an upstream residual SPM flux

$$\mathbf{F}_c = \frac{1}{T}\int_T (uC,\ (w - w_s)C - \nu_t'\partial_z C)\ dt \qquad (32)$$

with a maximum at x = 38 km and z = −8 m (see Fig. 5).

It cannot be estimated at this stage which of the mechanisms (i) and (ii) decribed above is mainly responsible for the residual countercurrent. It is not clear even if additional (e.g., barotropic) mechanisms are important. In order to investigate this, experiments 2 and 3 are performed, one excluding (i) residual gravitational circulation and the other excluding (ii) tidal velocity asymmetry.

b. Experiments with reduced physics

An inspection of the results of experiment 2 where the (i) residual gravitational circulation has been excluded shows that there is an accelerating outflow of tidal mean total SPM content

$$C_{\text{tot}} = \frac{1}{T}\int_T \int_0^L \int_{-H}^{\zeta} C\ dz\ dx\ dt \qquad (33)$$

out of the estuary after 15 tidal periods (see Fig. 9). Figure 3b illustrates that an ETM is initially developing but after a while (20 tides) decreasing again. The reason for this is that the near-bottom residual countercurrent is now significantly weaker than in experiment 1 (see Fig. 7). The maximum value of the residual countercurrent is less than 0.015 m s^{-1}. It can be concluded from this that the (i) residual gravitational circulation is a necessary mechanism for the formation of a stable ETM in the idealized estuary considered in this paper.

In experiment 3, where the (ii) tidal velocity asymmetry has been excluded, no residual countercurrent is developing in the whole estuary (see Fig. 8). A much weaker ETM than in experiment 2 is initially developing but breaking down after only a few tidal phases, which is reflected by the strong decrease of total SPM in the estuary (see Fig. 9). In both experiments 2 and 3 the initial development of an ETM is caused by the remaining mechanism still included in the physics. It can be concluded in the context considered here that both the (i) residual gravitational circulation and the (ii) tidal velocity asymmetry contribute significantly to the establishment of a residual countercurrent. Furthermore, the influence of the latter mechanism appears to be more important in the setup considered here.

The third ETM generation mechanism mentioned above, the (iii) tidal mixing asymmetry, is not responsible for the residual countercurrent but may nevertheless be necessary for the formation of an ETM. It is clear that this mechanism included in experiment 2 and only partially in experiment 3 is not sufficient for the formation of a stable ETM. In this final experiment 4, the same hydrodynamic situation as in experiment 1 is considered, that is, the same residual currents as shown in Fig. 4 are transporting the SPM. Although the (iii) *tidal mixing asymmetry* is neglected by means of using a constant eddy diffusivity for the vertical SPM mixing, a stable ETM is formed that is weaker than in experiment 1 (see Fig. 3d). Due to the exponential SPM profiles resulting from a constant sinking speed and diffusivity, there is a near-bottom upstream transport of SPM in the area of the salt wedge. The small outflow of SPM even after 30 tidal periods (see Fig. 9) may be due to the fact that significant SPM concentrations remain high up in the water column where no countercurrent exists. This effect is similar to the presence of a small sinking speed. Nevertheless, the stability of the ETM seems not to be very sensitive to the vertical mixing of SPM. This is an a posteriori argument for the fact that the quality of the turbulence model is not decisive for the modeling of ETMs in principal. However, having chosen the well-tested k–ε model gives this study an enhanced reliability.

6. Conclusions

The formation of estuarine turbidity maxima related to density effects in the salt wedge have been investigated by means

of a 2D (*xz*) model applied to an idealized situation typical for a macrotidal estuary. Three different mechanisms, namely (i) the residual gravitational circulation, (ii) the tidal velocity asymmetry, and (iii) the tidal mixing asymmetry are discussed. With all three effects considered commonly, a stable ETM is established within a few tidal periods. It could be shown that a near-bottom residual countercurrent in the region of the salt wedge was responsible for the upstream transport of SPM. The neglect of one of the mechanisms (i) or (ii) resulted in a weakened [neglect of (i)] or vanished [neglect of (ii)] residual near-bottom countercurrent and therefore in a significant outflow of SPM through the open sea boundary. As a consequence of that, a stable ETM did not become established. It turned out that in the situation considered in this paper, mechanism (ii) was significantly more relevant than (i).

Mechanism (iii) proved to cause an additional upstream transport of SPM, although it was, in contrast to the two other mechanisms, not necessary for the formation of a stable ETM.

It can be concluded from the results obtained that near-bottom gradients play a dominant role for the formation of an ETM. Therefore, the discretization in this region has to be carried out carefully. A coarse vertical resolution could significantly underestimate the residual countercurrent. Similar problems would arise if the bottom is sloping and non-terrain-following coordinates (such as *z* coordinates) are used, which introduce discrete steps at the bottom.

It could be shown by means of these idealized experiments that the formation of an ETM does not require specific features like a bottom bathymetry, form of the coastline, or internal SPM sources. Furthermore, the stability of an ETM seems to be insensitive to particle sizes, particle concentration, or cohesive effects. The total SPM content converged for this periodically stationary, flat-bottom estuary to a tidal mean steady state. It can be concluded from this that in a large variety of macrotidal estuaries, SPM can be trapped in the estuary for a long time.

Acknowledgments

This work has initially been funded jointly by Deutsche Forschungsgemeinschaft/Sonderforschungsbereich 327 ‘Tide-Elbe’ and GKSS Forschungszentrum. Fortunately, further support has been granted by the Danish Research Foundation and by the European MAST project PROMISE. Their support was essential and is greatly appreciated. We further want to thank Susanne Rolinski and Jürgen Sündermann in Hamburg for interesting and helpful discussions.

REFERENCES

Allen, G. P., C. Salomon, P. Bassoullet, Y. Du Penhoat, and C. De Grandpre’, 1980: Effects of tides on mixing and suspended sediment in macrotidal estuaries. *Sediment Geol.,* **26,** 69–80..

Ariathurai, R., and R. B. Krone, 1976: Mathematical modelling of sediment transport in estuaries. *Estuarine Processes.* Vol. II, M. Wiley, Ed., Academic Press, 98–106..

Backhaus, J. O., 1985: A three-dimensional model for the simulation of shelf sea dynamics. *Dtsch. Hydrogr. Z.,* **38,** 165–187..

Baumert, H., and G. Radach, 1992: Hysteresis of turbulent kinetic energy in nonrotational tidal flows: A model study. *J. Geophys. Res.,* **97,** 3669–3677..

— ,~~,~~G. Bruckner, E. Kleine, R. Kluge, W. Müller, and S. Unger, 1989: Numerical simulation of estuarine hydrodynamics. *Syst. Anal. Model. Simul.,* **6,** 503–506..

Brørs, B., and K. J. Eidsvik, 1994: Oscillatory boundary layer flows modelled with dynamic Reynolds stress turbulence closure. *Contin. Shelf Res.,* **14,** 1455–1475..

Burchard, H., 1995: Turbulenzmodellierung mit Anwendungen auf thermische Deckschichten im Meer und Strömungen in Wattengebieten, Ph.D. thesis, GKSS Research Centre Geesthacht, Geesthacht, 299 pp. [Available from Dr. Hans Burchard, Joint Research Centre, Space Applications Institute, TP 690, I-21020 Ispra (Va), Italy.].

— ,~~a~~nd H. Baumert, 1995: On the performance of a mixed-layer model based on the *k*–~~E~~ turbulence closure. *J. Geophys. Res.,* **100,** 8523–8540..

Casulli, V., and R. T. Cheng, 1992: Semi-implicit finite difference methods for three-dimensional shallow water flow. *Int. J. Num. Meth. Fluids,* **15,** 629–648..

Dammschneider, H.-J., 1992: Der Unterelbe-Salzkeil—Eine morphodynamische Bewertung, *Die Küste—Archive for Research and Technology on the North Sea and Baltic Coast,* Vol. 53, 29–50. (Engl. summary).

Festa, J. F., and D. V. Hansen, 1976: A two-dimensional numerical model of estuarine circulation: The effects of altering depth and river discharge. *Estuar. Coastal Mar. Sci.*, **4,** 309–323..

— , and — , 1978: Turbidity maxima in partially mixed estuaries. *Estuarine Coastal Mar. Sci.*, **7,** 347–359..

Fischer, H. B., 1972: Mass transport mechnisms in partially stratified estuaries. *J. Fluid Mech.*, **53,** 671–687..

Flather, R. A., 1976: A tidal model of the northwest European continental shelf. *Mem. Soc. R. Sci. Liege*, **10,** 141–164..

Geyer, W. R., 1993: The importance of suppression of turbulence by stratification on the estuarine turbidity maximum. *Estuaries*, **16,** 113–125..

Gill, A. E., 1982: *Atmosphere–Ocean Dynamics.* Academic Press, 662 pp..

Ionello, J. P., 1979: Tidally induced residual currents in estuaries of variable breadth and depth. *J. Phys. Oceanogr.*, **9,** 962–974..

Jay, D. A., and J. D. Musiak, 1994: Particle trapping in estuarine tidal flows. *J. Geophys. Res.*, **99**(20), 445–461..

Kausch, H., and W. Michaelis, Eds., 1996: Suspended particulate matter in rivers and estuaries. *Adv. Limnol.*, **47,** 573 pp..

Krone, R. B., 1992: Flume studies of the transport of sediment in estuarial shoaling processes. Final Report, Hydraulic Eng. Lab U.S. Army Corps of Eng., 110 pp. [Available from U.S. Army Engineer Waterways Experiment Station, Vicksburg, MS 39180.].

Lang, G., R. Schubert, M. Markowsky, H.-U. Fanger, I. Grabemann, H. L. Krasemann, L. J. R. Neumann, and R. Riethmüller, 1989:Data interpretation and numerical modelling of the Mud and Suspended Sediment Experiment 1985. *J. Geophys. Res.*, **94,** 14381–14393..

Launder, B. E., and D. B. Spalding, 1972: *Mathematical Models of Turbulence.* Academic Press, 169 pp..

Le Bris, H., and M. Glémarec, 1996: Marine and brackish ecosystems of South Brittany (Lorient and Vilaine bays) with particular reference to the effect of the turbidity maxima. *Estuarine, Coastal Shelf Sci.*, **42,** 737–753..

Lindsay, P., P. W. Balls, and J. R. West, 1996: Influence of tidal range and river discharge on suspended particulate matter fluxes in the Forth estuary. *Estuarine Coastal Shelf Sci.*, **42,** 63–82..

Lobmeyr, M., and W. Puls, 1991: Modellrechnungen zum Schwebstofftransport: Vergleich der Ergebnisse eines zweidimensionalen Modells mit Feldmessungen im Elbästuar. Report GKSS 91/E/25, GKSS Research Centre Geesthacht, Geesthacht, 53 pp. [Available from GKSS Research Centre, D-21494 Geesthacht, Germany.].

Marchuk, G. I., V. P. Kochergin, V. I. Klimok, and V. A. Sukhorukov, 1977: On the dynamics of the ocean surface mixed layer. *J. Phys. Oceanogr.*, **7,** 865–875..

Michaelis, W., Ed., 1990: *Estuarine Water Quality Management: Modelling, Monitoring and Research.* Springer-Verlag, 478 pp..

Munk, W. H., and E. R. Anderson, 1948: Notes on the theory of the thermocline. *J. Mar. Res.*, **3,** 276–295..

Omstedt, A., J. Sahlberg, and U. Svensson, 1983: Measured and numerically-simulated autumn cooling in the Bay of Bothnia. *Tellus*, **35A,** 231–240..

Patankar, S. V., 1980: *Numerical Heat Transfer and Fluid Flows.* McGraw-Hill, 197 pp..

Postma, H., and K. Kalle, 1955: Die Entstehung von Trübungszonen im Unterlauf der Flüsse, speziell im Hinblick auf die Verhältnisse in der Unterelbe. *Dtsch. Hydrogr. Z.*, **8,** 137–144..

Rodi, W., 1980: Turbulence models and their application in hydraulics. Int. Assoc. for Hydraul. Res. Rep. Delft, the Netherlands, 104 pp. [Available from International Association for Hydraulic Research, Rotterdamseweg 185, P.O. Box 177, 2600 MH Delft, the Netherlands.].

— , 1987: Examples of calculation methods for flow and mixing in stratified flows. *J. Geophys. Res.*, **92,** 5305–5328..

Schröder, M., and G. Siedler, 1989: Turbulent momentum and salt transport in the mixing zone of the Elbe estuary. *Estuarine Coastal Shelf Sci.*, **28,** 615–638..

Simenstad, C. A., D. J. Reed, D. A. Jay, J. A. Baross, F. G. Prahl, and L. F. Small, 1994: Landmargin ecosystem research in the Columbia River estuary: An interdisciplinary approach to investigating couplings between hydrological, geochemical and ecological processes within estuarine turbidity maxima. *Changes in Fluxes in Estuaries: Implications from Science to Management*, K. R. Dyer and R. J. Orth, Eds., Olsen & Olsen, 437–444..

van de Kreeke, J., 1996: Net transport of fine sediment in a homogeneous tidal channel. *Mixing in Estuaries and Coastal Seas, Coastal and*

Estuarine Studies 50, Amer. Geophys. Union, 361–373..

van Leussen, W., 1988: Aggregation of particles, settling velocity of mud flocs: A review. *Physical Processes in Estuaries*, J. Dronkers and W. van Leussen, Eds., Springer-Verlag, 347–403..

Wellershaus, S., 1981: Turbidity maximum and shoaling in the Weser estuary. *Arch. Hydrobiol.*, **92,** 161–198..

Zalesak, S. T., 1979: Fully multidimensional flux-corrected transport algorithms for fluids. *J. Comput. Phys.*, **31,** 335–362..

Tables

Table 1. Empirical constants for the standard κ–ϵ model.

Parameter	Value
c_μ	0.09
c_1	1.44
c_2	1.92
c_3	−1.4
σ_κ	1.00
σ_ϵ	1.30

Click on thumbnail for full-sized image.

Table 2. Parameters for the numerical experiments.

Parameter	Value	Unit
B_0	0.3	kg m^{-2}
c_ϵ	0.5	kg s m^{-1}
c_m	2×10^{-5}	m^{-2}
g	9.81	m s^{-2}
H	15	m
K_v	0.2	m
L	100 000	m
ν	1.3×10^{-6}	m^{2}s^{-1}
ν'	1.1×10^{-9}	m^{2}s^{-1}
ν''	1×10^{-5}	m^{2}s^{-1}
ν'_0	0.005	m^{2}s^{-1}
ρ_0	999.725	kg m^{-3}
S_{max}	30	psu
T	44714	s
t_0	1800	s
τ_{cr}	0.13	kg m^{-1}s^{-2}
τ_{cr}	0.1	kg m^{-1}s^{-2}
u_0	1.5	m s^{-1}
u_r	0.05	m s^{-1}
w_s	0.001	m s^{-1}
x_m	20 000	m
ζ_0	1.3	m

Click on thumbnail for full-sized image.

Figures

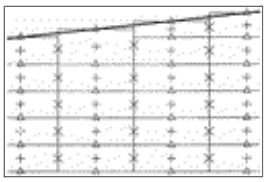

Click on thumbnail for full-sized image.

Fig. 1. Sketch of the staggered grid. Bold line: free surface; +: SPM and salinity; ×: u; Δ: w, k, ϵ, ν_t, and ν'_t.

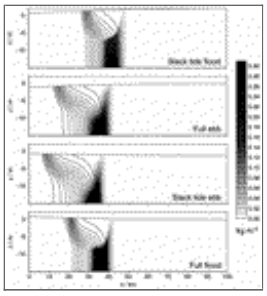

Click on thumbnail for full-sized image.

Fig. 2. Instantaneous salinity and SPM distribution for four different tidal phases. Leftmost salinity isoline: 28 psu, rightmost salinity isoline: 2 psu, interval 2 psu. The tidal phases are defined as follows. Full ebb: maximum negative bottom velocity at x = 40 km; full flood:maximum positive bottom velocity at x = 40 km; slack tide ebb: minimum water level at x = 40 km; slack tide flood:

maximum water level at x = 40 km.

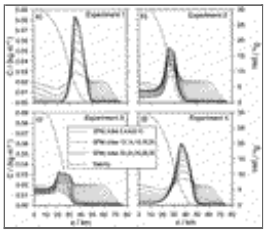

Click on thumbnail for full-sized image.

Fig. 3. Tidal mean vertically averaged SPM concentrations for 15 different tides and tidal mean vertically averaged salinity. The curves are shown for all four experiments.

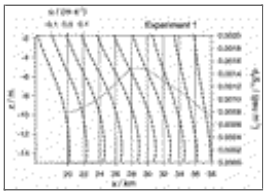

Click on thumbnail for full-sized image.

Fig. 4. Experiment 1: Tidal mean velocity profiles at 10 longitudinal locations in regions of the salt wedge. Each profile is shown with respect to a vertical axis placed at the position where the profile was calculated. Dashed: Horizontal gradient of tidal mean vertically averaged salinity.

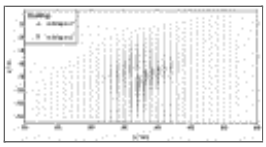

Click on thumbnail for full-sized image.

Fig. 5. Experiment 1: Vector plot of tidal mean SPM fluxes, F_c in the salt wedge.

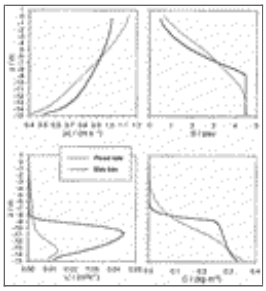

Click on thumbnail for full-sized image.

Fig. 6. Experiment 1: Vertical profiles for full flood (bold line) and full ebb (thin line) at a location where the vertically averaged salinity is $\overline{S}$ = 3 psu. Upper left: modules of horizontal velocities; upper right: salinities; lower left: eddy diffusivities; lower right: SPM concentrations.

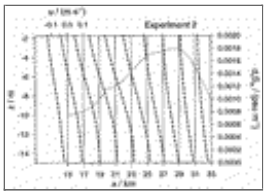

Click on thumbnail for full-sized image.

Fig. 7. Same as Fig. 4 but for experiment 2.

Click on thumbnail for full-sized image.

Fig. 8. Same as Fig. 4 but for experiment 3.

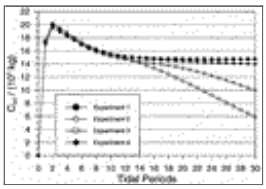

Click on thumbnail for full-sized image.

Fig. 9. Tidal mean values of total SPM contents, C_{tot}, of the model domain in the four experiments as a function of time.

Corresponding author address: Dr. Hans Burchard, Joint Research Centre, Space Applications Institute, TP 690, I-21020 Ispra (Va), Italy.
E-mail: hans.burchard@jrc.it

top